

Article

Effect of Additives on the Morphologies of Hydrothermal Products Prepared from Semi-Dry Desulfurization Residues

Lixia Li , Haiqing Hao * and Zhitao Yuan

School of Resources & Civil Engineering, Northeastern University, Shenyang 110819, China; lilixia@mail.neu.edu.cn (L.L.); yuanzhitao@mail.neu.edu.cn (Z.Y.)

* Correspondence: yesterday1019@163.com; Tel.: +86-024-8368-7694

Received: 1 September 2018; Accepted: 3 November 2018; Published: 6 November 2018



Abstract: For effective utilization of the residues, calcium sulfate whiskers were prepared from semi-dry desulfurization residues by hydrothermal synthesis reactions. Aiming at collecting the products with a long length and large aspect ratio, the additives, including sodium oleate, sodium dodecyl benzene sulfonate (SDBS), and sodium citrate, were added to control the growth of the crystal. Compared with no additives, whiskers with relatively a longer length and larger aspect ratio could be obtained in the presence of sodium oleate or SDBS. The sodium citrate made the whiskers thicker and shorter. Then, the effects of the additives on crystal growth and the morphology of the hydrothermal products were investigated with the aid of X-ray diffraction (XRD) patterns and molecular dynamics simulations. According to the results of XRD, the diffraction intensity of the crystal face (400) increased under the influence of sodium oleate, promoting crystal growth along the c-axis. The molecular structures of the corresponding faces were built based on the strong peaks shown in the XRD patterns. The atomic distribution on the computed crystal faces was presented. The interaction energies on different faces were calculated to illustrate the different adsorption configurations of the additives. Among the calculated faces, the interaction energies on (400) were both most negative for sodium oleate and SDBS. Therefore, sodium oleate and SDBS preferred to adsorb on (400). As a result, the growth of (400) was thus inhibited and the crystal grew along the c-axis. Compared with sodium oleate and SDBS, the lowest adsorption energy of sodium citrate on the face (310) indicated that sodium citrate has no positive effect on the directional growth of the crystal parallel to c-axis. The molecular simulation results were virtually identical to the crystal faces analysis results.

Keywords: semi-dry desulfurization residues; additives; crystal faces; molecular dynamics simulations

1. Introduction

Semi-dry desulfurization residues, which are the main byproducts of the semi-dry flue gas desulfurization (FGD) process, are a mixture of CaSO_4 , CaSO_3 , and CaO [1,2]. Coal-fired power plants currently produce tons of semi-dry desulfurization residues each day, so the problem of their utilization has become a focus of attention [3]. Much research has been conducted into utilizing the residues as cement retarders, soil amendments, and building materials [4–9]. However, desulfurization residue has a complex composition with a high content of sulfur and relatively high CaSO_3 content, which seriously limits their applications [10]. The residue is typically stockpiled without any treatment, which could be a pollution threat to the environment [11]. Thus, profitably utilizing the large volume of these residues is vital for the sustainable development of coal-fired power plants. As a result of the high content of calcium, desulfurization residues have been used to produce gypsum or to prepare calcium

sulfate whiskers after pretreatment [12–17]. Sun et al. synthesized calcium sulfate whiskers from the FGD gypsum using the atmospheric acidification method [18]. However, for efficient utilization of large volumes of desulfurization residues, hydrothermal synthesis is a promising approach. Wang et al. prepared calcium sulfate whiskers from purified FGD gypsum and investigated the morphology and phase structure of the hydrothermal products in the $\text{H}_2\text{SO}_4\text{-NaCl-H}_2\text{O}$ system [19]. Products of calcium sulfate hemihydrate were obtained.

The calcium sulfate whisker is a promising reinforcing material with a high aspect ratio [20]. Because of the remarkable advantages of high tensile strength and elastic modulus, calcium sulfate whiskers are often applied in rubber, paper, plastics, and ceramics as fillers to improve the comprehensive properties, including thermal stability, mechanical strength, chemical resistance, and electrical insulation [21–24]. The physical properties of the materials are highly dependent on the morphology of the whiskers [25]. The ones that have morphologies with smooth surfaces and fine sizes show outstanding insulation properties and chemical resistance [26]. Therefore, care was taken to control the crystal growth and the morphology, in order to improve the performance and application of the calcium sulfate whiskers. Organic reagents can promote or inhibit the crystal growth along specific planes to modify the morphology [27]. Liu et al. investigated the effects of particle size of FGD gypsum, slurry concentration, and additives on calcium sulfate whiskers prepared from FGD gypsum [28,29]. The results indicated that sodium dodecyl benzene sulfonate could improve the morphology of the calcium sulfate whiskers. Yang et al. analyzed the effects of citric acid and sodium oleate on the preparation of calcium sulfate and explored the adsorption mechanisms of the additives via thermogravimetry and differential scanning calorimetry (DSC-TG) analysis [30]. However, they did not consider the face structures of the whiskers.

Research has revealed that the modification mechanism of the additives on the morphology of calcium sulfate whiskers was due to the selective adsorption of the additives onto different crystal faces [31–33]. The molecular simulation technique appears to be a promising method of evaluating the interactions at interfaces and has been widely used to examine the details of crystal structures and the interactions between additives and crystal faces [34–37]. Yin et al. studied the intermolecular contact between additives and the crystal faces of salbutamol sulfate and concluded that molecular dynamics simulation was a powerful tool in terms of the selection of additives for crystallization [38]. Mao et al. studied the effects of sodium dodecyl sulfonate and sodium dodecylbenzene sulfonate on the morphology of calcium sulfate hemihydrate through experiments in aqueous system molecular dynamics simulations. They also concluded that molecular dynamics simulation is helpful in performance evaluation and in modifier selection [39].

For effective utilization of the semi-dry desulfurization residues, the synthesis of calcium sulfate whiskers was explored using hydrothermal methods. Different additives, including sodium oleate, sodium dodecyl benzene sulfonate (SDBS), and sodium citrate, were added to investigate the effects of additives on the morphologies of the hydrothermal products. The molecular structures of the predominant faces were built and the adsorption configurations of the additives on different faces were computed based on the faces determined by the X-ray diffraction (XRD) of the products. Thus, the growth of the calcium sulfate whiskers prepared from the semi-dry desulfurization residues could be controlled by different additives and the residues could ultimately be utilized properly and efficiently.

2. Materials and Methods

2.1. Materials

The semi-dry desulfurization residues were collected from a power plant of the Anshan Iron and Steel Group Corporation (AISG). First, the desulfurization residues were pretreated with dilute sulfuric acid solution. Samples with 92% calcium sulfate were thus obtained. Sulfuric acid (H_2SO_4 , 95–98%, Liaoning Minsheng Chemical Co. Ltd., Shenyang, China) and sodium citrate ($\text{C}_6\text{H}_5\text{Na}_3\text{O}_7 \cdot 2\text{H}_2\text{O}$, 90%, Tianjin Bodi Chemical Co. Ltd., Tianjin, China) were analytically pure. Sodium oleate ($\text{C}_{18}\text{H}_{33}\text{NaO}_2$,

98%, Sinopharm Chemical Reagent Co. Ltd., Shanghai, China) and sodium dodecyl benzene sulfonate ($C_{18}H_{29}NaO_3S$, 90%, Shenyang Licheng Chemical Reagent Factory, Shenyang, China) were chemically pure.

2.2. Preparation of Calcium Sulfate Whiskers

The hydrothermal synthesis method was adopted to prepare calcium sulfate whiskers with and without additives. A high-pressure reactor with an inside diameter of 213 mm, an outside diameter of 225 mm, and a height of 600 mm was employed for the synthesis. The mixing blades and heating devices were set up inside the reactor. A temperature controller was used to regulate the temperature during the reaction. The semi-dry desulfurization residues were pre-treated by a sulfuric acid solution with a volume concentration of 20%. The concentration was the same as that of the waste acid in the power plant. Further research on utilizing waste acid in the synthesis process will be conducted. Residue slurry for the hydrothermal synthesis was prepared using 250 g of pre-treated residues. The mass concentration was set at 3%. On the basis of the results of the previous exploratory experiments, the mass ratio of the additives to the mass of the residues was set at 0.15%, 0.1%, and 0.1% for sodium oleate, SDBS, and sodium citrate, respectively. After the additives were added, the pH value of the slurry was adjusted to 9.25 and then the conditioned slurry was poured into the high-pressure reactor. The autoclave body was heated and then kept at 120 °C for 120 min, which was also determined via the exploratory experiments. The gas pressure in the reactor rose as the temperature rose and finally remained stable. At the end of the reaction, the gas with pressure was released. The hydrothermal products would be rapidly taken out, dehydrated, and dried as soon as the gas pressure of the reactor decreased to the normal atmospheric pressure.

2.3. Characterization of the Hydrothermal Products

The product was spread on a glass slide with the help of absolute ethanol. After the ethanol evaporated away completely, the slide was observed under the scope of an inverted microscope (BDS200, Chongqing Optec Instrument Co. Ltd., Chongqing, China). The captured images were then transferred to an implemented image processing software (Runzhi Tech Co. Ltd., Jinan, China), by which the lengths and diameters of the sampled products were measured and recorded, and the aspect ratios were calculated. For every product, 200 crystals were counted for the mean value. The morphology of the products was further observed by scanning electron microscopy (SEM, SSX-550, Shimadzu, Kyoto, Japan).

The XRD patterns were obtained by an X'Pert Pro diffractometer (X'Pert Pro MPDDY2094, PANalytical B.V., Almelo, The Netherlands), which was operated at 40 kV, 30 mA, with a diffraction angle range of 2θ from 5° to 90° by Cu $K\alpha$ radiation. Then, the obtained XRD patterns were imported to MDI Jade software for spectra fitting and crystal face analysis. After phase retrieval, both phases and faces were compared with the database and it was noted that the No. 79529 PDF card matched the experimental XRD patterns well.

2.4. Details of Molecular Dynamics Simulations

The adsorption of the additives on different crystal faces was analyzed through the molecular dynamics simulation method. All the simulations were conducted in the Forcite module and the condensed-phase optimized molecular potentials for atomistic simulation studies (COMPASS) force field with the software package Materials Studio 7.0 (Asselrys Inc., San Diego, CA, USA).

The functional forms used in the COMPASS force field are as follows [40]:

$$E = E_{bond} + E_{angle} + E_{oop} + E_{torsion} + E_{cross} + E_{elec} + E_{vdW} \quad (1)$$

$$E_{bond} = \sum_b \left[k_2(b - b_0)^2 + k_3(b - b_0)^3 + k_4(b - b_0)^4 \right] \quad (2)$$

$$E_{angle} = \sum_{\theta} [H_2(\theta - \theta_0)^2 + H_3(\theta - \theta_0)^3 + H_4(\theta - \theta_0)^4] \quad (3)$$

$$E_{torsion} = \sum_{\theta} [V_1 [1 - \cos(\phi - \phi_0)]^2 + V_2 [1 - \cos(2\phi - \phi_0)]^2 + V_3 [1 - \cos(3\phi - \phi_0)]^2] \quad (4)$$

$$E_{oop} = \sum_{\chi} k_{\chi} \chi^2 \quad (5)$$

$$\begin{aligned} E_{cross} = & \sum_b \sum_{b'} F_{bb'}(b - b_0)(b' - b'_0) + \sum_{\theta} \sum_{\theta'} F_{\theta\theta'}(\theta - \theta_0)(\theta' - \theta'_0) \\ & + \sum_b \sum_{\theta} F_{b\theta}(b - b_0)(\theta - \theta_0) \\ & + \sum_b \sum_{\phi} F_{b\phi}(b - b_0)[V_1 \cos \phi + V_2 \cos 2\phi + V_3 \cos 3\phi +] \\ & + \sum_{b'} \sum_{\phi} F_{b'\phi}(b' - b'_0)[V_1 \cos \phi + V_2 \cos 2\phi + V_3 \cos 3\phi +] \\ & + \sum_{\theta} \sum_{\phi} F_{\theta\phi}(b - b_0)[V_1 \cos \phi + V_2 \cos 2\phi + V_3 \cos 3\phi +] \\ & + \sum_{\theta} \sum_{\theta'} \sum_{\phi} k_{\phi\theta\theta'} \cos \phi F_{b\phi}(\theta - \theta_0)(\theta' - \theta'_0) \end{aligned} \quad (6)$$

$$E_{elec} = \sum_{i,j} \frac{q_i q_j}{\epsilon r_{ij}} \quad (7)$$

$$E_{vdW} = \sum_{i,j} \epsilon_{ij} \left[2 \left(\frac{r_{ij}^0}{r_{ij}} \right)^9 - 3 \left(\frac{r_{ij}^0}{r_{ij}} \right)^6 \right] \quad (8)$$

where E_{bond} , E_{angle} , E_{oop} , $E_{torsion}$, E_{cross} , E_{elec} , and E_{vdW} denote the energy of bond stretching, angle bending, out of plane angle coordinates, torsion, cross-coupling, electrostatic, and van der Waals, respectively. b , θ , ϕ , and χ represent bond lengths, bond angles, torsion angles, and out of plane angles, respectively.

The XRD patterns of hydrothermal products matched the No. 79529 PDF card well, and the unit cell model of the products, in which the main phase was calcium sulfate hemihydrates ($\text{CaSO}_4 \cdot 0.5\text{H}_2\text{O}$), was constructed. This is a monoclinic crystal with a space group I121. The primitive structure showed that the cell parameters were $a = 12.0317 \text{ \AA}$, $b = 6.9269 \text{ \AA}$, $c = 12.6712 \text{ \AA}$, $\alpha = \gamma = 90^\circ$, and $\beta = 90^\circ 27'$ [41].

The geometry optimization was first performed on the unit cell. The morphologically apparent crystal faces (hkl) were obtained from the XRD patterns. Geometry optimization of the face models was carried out with the bottom atoms fixed. Supercells were established with the optimized crystal faces. To build the initial configurations of adsorption for further investigation, additive molecules that may react with the atoms on crystal faces needed to be optimized geometrically before being put on the crystal faces. The adsorption configuration was optimized to obtain the best position in a state of adsorption equilibrium using the Smart algorithm with a convergence level of 0.001 Kcal/mol. The group-based summation method and the Ewald summation method with ultrafine calculation accuracy were used to calculate the van der Waals force and electrostatic energy, respectively. Atomic charges were calculated by the charge equilibration (QEq) method [42]. Molecular dynamics simulations were then performed to make the configuration energy converge. Molecular dynamics simulation with a velocity scale thermostat was used to obtain the initial velocity of the configuration. An essential molecular dynamics simulation with an NVT ensemble (In the system, the particle number N , volume V , and temperature T are kept constant) was then carried out on at the nose thermostat at 393 K with a time step of 1 fs and a total simulation time of 50 ps. Configuration with the lowest energy is the optimal model of adsorption, with which the calculation of interaction energy was based on. The interaction energy was obtained by the following formula [38]:

$$\Delta E = E_{total} - E_{additive} - E_{crystal} \quad (9)$$

where ΔE is the interaction energy; and E_{total} , $E_{additive}$, and $E_{crystal}$ are the total energy of the model, the energy of the additive, and the energy of the crystal, respectively.

The value of the interaction energy demonstrates the stability of the adsorption system. The more negative the value, the more stable the system. The additive could thus easily be adsorbed on the crystal faces. If the interaction energy is zero or even positive, the additive could not adsorb on the crystal faces [43].

3. Results and Discussion

3.1. Effect of Additives on the Morphology of the Products

Figure 1 shows the images of the hydrothermal products with and without additives. Compared with the products without additives, the length increased while the diameter decreased after sodium oleate and SDBS were added separately. When it comes to the products with sodium citrate, short columns with a large diameter were obtained. Combining the length and the aspect ratio shown in Figure 2, the calcium sulfate whiskers with an average length of 89 μm and an aspect ratio of 29.67 were obtained in the absence of additives. Both the length and the aspect ratio increased after sodium oleate or SDBS was added. Specifically, calcium sulfate whiskers with a length of 125 μm and an aspect ratio of 41.67 were obtained when 0.1% SDBS was added. They were the longest and thinnest among the four products. When 0.15% sodium oleate was added, whiskers with a length of 112 μm and an aspect ratio of 40 were obtained. However, when 0.1% sodium citrate was added, the thickness of the whiskers increased and the average aspect ratio decreased to 21.05.

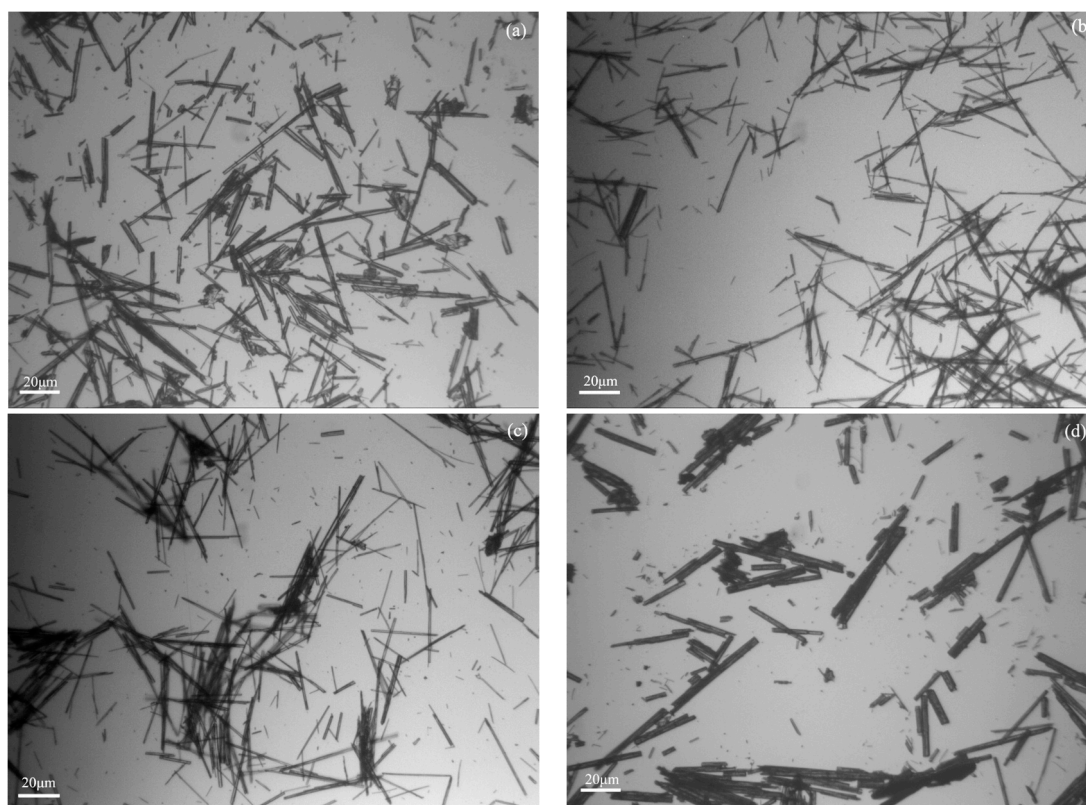


Figure 1. Images of the synthesized products (a) without additives and in the presence of (b) sodium oleate, (c) sodium dodecyl benzene sulfonate (SDBS), and (d) sodium citrate.

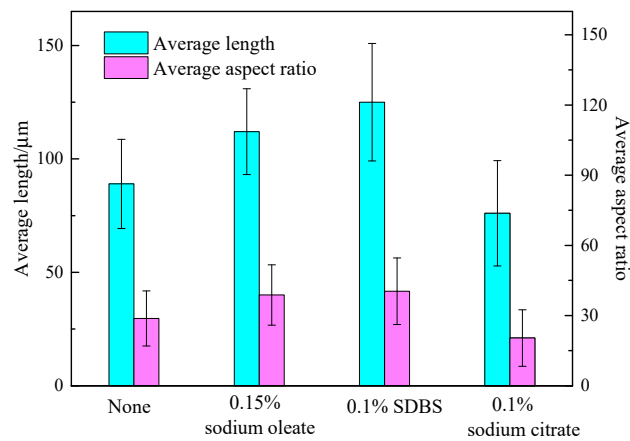


Figure 2. Average length and aspect ratio of the synthesized products.

Figure 3 shows the SEM images of the products for detailed morphologies of the products. In Figure 3a, the shape of the prepared crystals was nearly columnar with smooth surfaces and flat cross-sections in the absence of additives. When sodium oleate or SDBS was added, more slender products were synthesized. Furthermore, some of them were in the fascicular form because of the insufficient dispersion. With the addition of the additives, the cross-sections demonstrated obvious irregular dentate shapes. When sodium citrate was added, the hydrothermal products presented short-column and fascicular shapes. It could be deduced that sodium citrate could not improve the growth of the calcium sulfate whiskers.

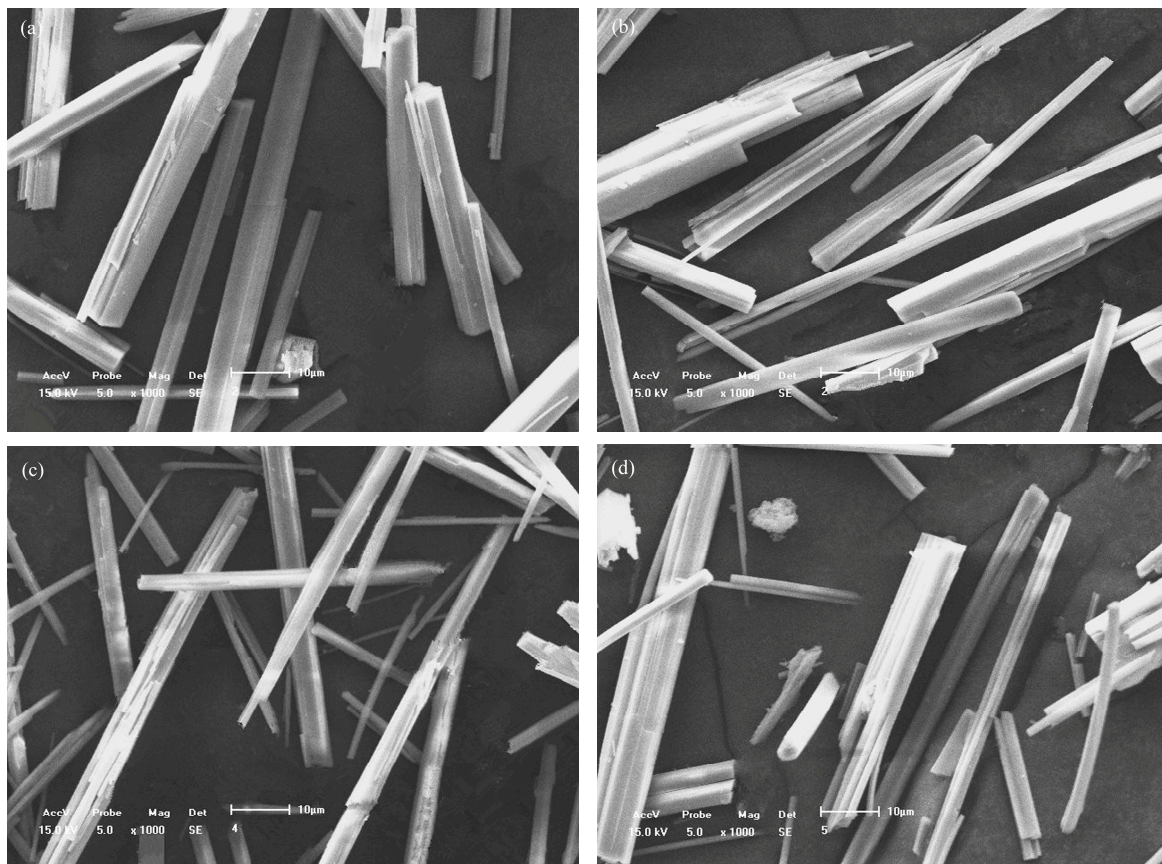


Figure 3. Morphologies of the synthesized products (a) without additives and in the presence of (b) sodium oleate, (c) SDBS, and (d) sodium citrate.

3.2. XRD Patterns of the Hydrothermal Products

It was verified that the additives could adsorb on specific crystal faces selectively, which prevented the adsorption of Ca^{2+} and SO_4^{2-} . Moreover, the additive molecules limited the movement of the ions. The products presented different morphologies due to the selective adsorption of the additives [44,45].

Figure 4 shows the XRD patterns of the hydrothermal products obtained without additives and with sodium oleate, SDBS, and sodium citrate, respectively. Different crystal faces were marked by the Miller indices. In the absence of additives, the diffraction strengths of (100), (200), and (110) were the top three peaks, as shown in Figure 4a. The crystal face (301), which is parallel with the b-axis, was the fourth strongest peak. The presence of (102), (201), and (301), showing the growth in the radial direction, was the main reason for the thick and short crystals. It should be noted that most products were in CaSO_4 phase, so that most faces corresponded with those of CaSO_4 crystal.

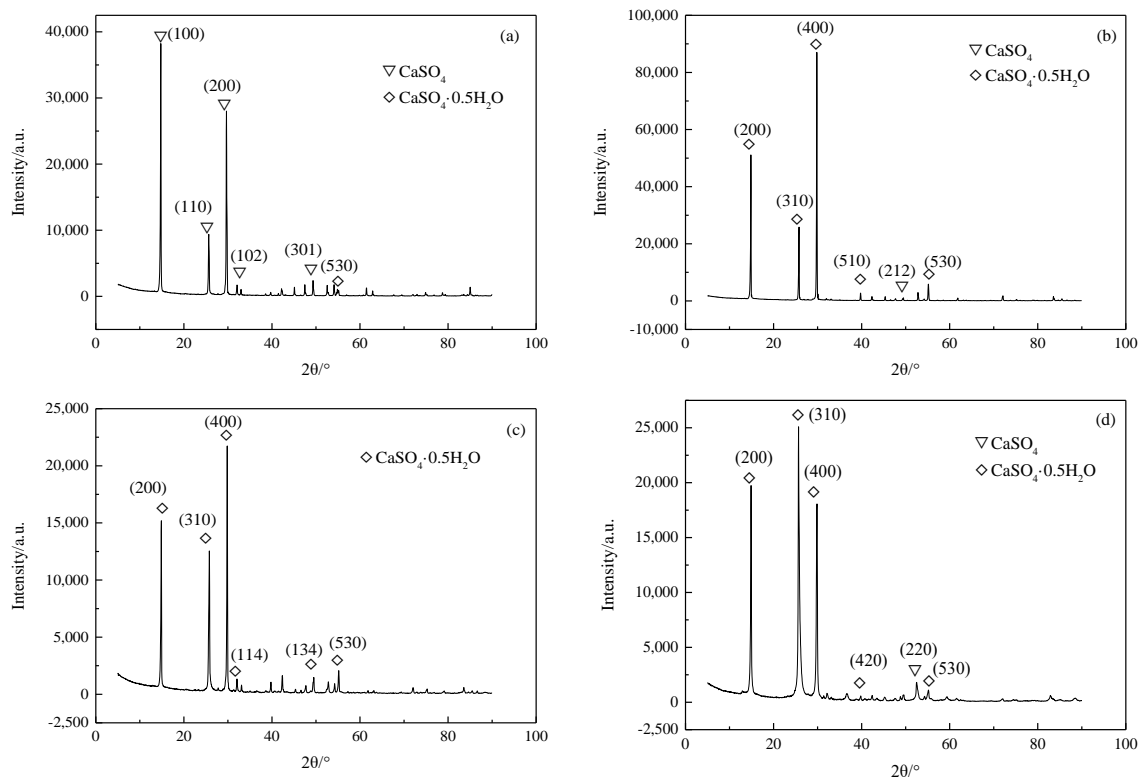


Figure 4. Diffraction strength of the crystal faces (a) with the absence of additives, (b) with sodium oleate, (c) with SDBS, and (d) with sodium citrate.

As for the hydrothermal products with sodium oleate, the diffraction strengths of (400) and (200), which were the top two peaks, both increased. The diffraction strength of (310), which was stronger than that of (530), was the third strongest. Obviously, the crystal growth along the c-axis was superior to that in the radial direction. The formation of calcium oleate on the crystal faces promoted the dissolution of dihydrate calcium sulfate, which in turn promoted the recrystallization of the hemihydrate calcium sulfate [46]. In addition, the formation and adsorption of the calcium oleate on (400) and (200) decreased the surface energies of the faces. The growth of the hydrothermal products along the c-axis was then accelerated. Ultimately, the aspect ratio of the hydrothermal products was increased. Therefore, sodium oleate could promote the crystal growth along the c-axis. With SDBS, the crystal faces of (400), (200), and (310) were the strongest peaks. Although the diffraction strength was lower than that with sodium oleate, the two had similar tendencies in terms of the face diffraction patterns, which might originate from the reaction between the organic acids and Ca^{2+} , and

the formation of stable compounds on the faces. The growth rate of the crystal faces was thus inhibited. The hydrothermal products grew along the *c*-axis.

As shown in Figure 4d, with sodium citrate, the crystal face of (310) was strengthened, whose diffraction strength was stronger than that of (200) and (400). It could be concluded that the crystals grew not only in the *c*-axis direction, but also in other directions. A combination of the perpendicular growth on the *c*-axis and along other directions made the hydrothermal products thick and short, which meant the faces in different directions had similar growth rates. As a result, most products eventually appeared in short columnar or even plate form. Thus, sodium citrate could not promote the synthesis of the calcium sulfate whiskers with a large aspect ratio.

3.3. Analysis of the Crystal Faces

The spectral fitting of the XRD patterns is summarized in Table 1. It could be seen that the calculated crystal parameters based on the experimental XRD patterns matched well with those in No. 79529 PDF card. Therefore, the molecular calculations on the referenced calcium sulfate hemihydrate ($\text{CaSO}_4 \cdot 0.5\text{H}_2\text{O}$) cells were reliable.

Table 1. Spectral fitting of X-ray diffraction (XRD) patterns.

Additives	Cell Parameters						R (%)
	<i>a</i> (Å)	<i>b</i> (Å)	<i>c</i> (Å)	α (°)	β (°)	γ (°)	
Sodium oleate	11.9079	6.9146	11.9118	90	90.23	90	10.77
SDBS	11.9558	7.1160	12.7695	90	91.90	90	9.85
Sodium citrate	11.9179	7.1357	12.7089	90	92.5	90	13.74

R describes the difference between the experimental observations and the ideal calculated values. SDBS represents sodium dodecyl benzene sulfonate.

As (200) and its harmonic (400) presented the same atomic distributions, it is rational to discuss the representative face of (400) for the face analysis and the interaction energy calculation [47,48]. On (400), regular distributions of calcium, oxygen, and hydrogen atoms indicated the similar adsorption of the calcium oleate and SDBS due to the similar carbon chain length and functional group. The steric hindrance caused by a long hydrocarbon chain prevented Ca^{2+} and SO_4^{2-} gathering at the crystal face [49]. Then, the growth of (400) was inhibited and thus the diffraction peak of (400) could be observed in Figure 4. Moreover, the growth could also be inhibited by sodium citrate to some extent. However, the differences in the growth rates of all the faces resulted in different crystal morphologies.

The face structure of (310) in Figure 5b shows that calcium ions located behind the first layer, which consisted of the oxygen atoms. The long hydrocarbon chain of the acid group, as shown in Figure 6, inhibited the complexation effects of sodium oleate and SDBS with the calcium ions. The sulfate ions, which are small molecules, could easily penetrate and adsorb on the face of (310). Thus, the growth of (310) could not be totally inhibited by calcium oleate and SDBS. However, the citric acid group of sodium citrate could penetrate and adsorb on the face through electrostatic adsorption, which prevented the growth of the face. Therefore, the diffraction peak of (310) could be observed in the XRD patterns. Thus, it was demonstrated that with sodium citrate, the diffraction strength of (310) was stronger than that of (400). Other faces such as (530) had weak interactions with the additives because few calcium ions and hydrogen atoms were distributed on the faces. Ultimately, these faces grew at specific rates.

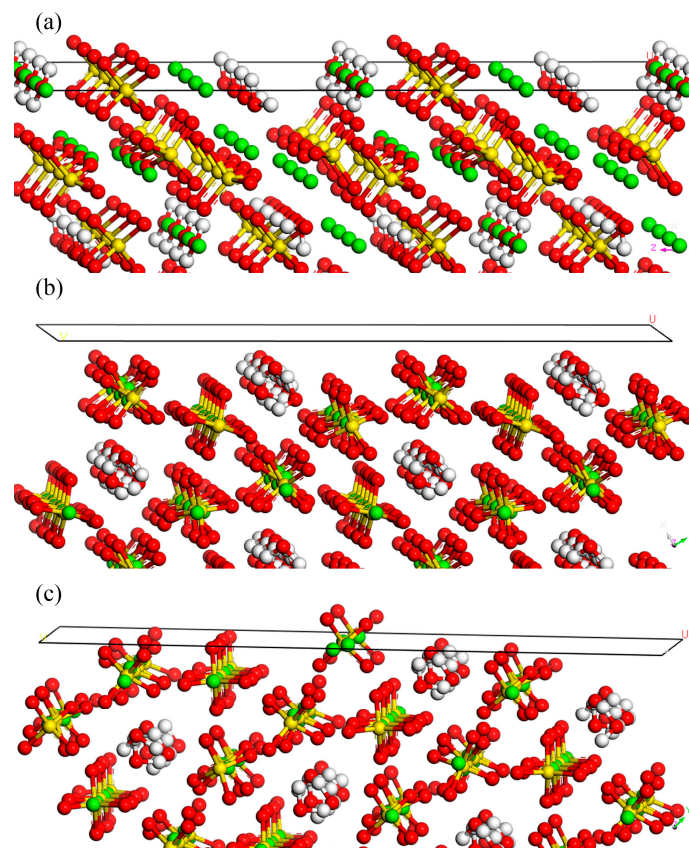


Figure 5. Structures of the crystal faces of (a) (400), (b) (310), and (c) (530). (Note: Red balls represent O. White balls represent H. Yellow balls represent S. Green balls represent Ca).

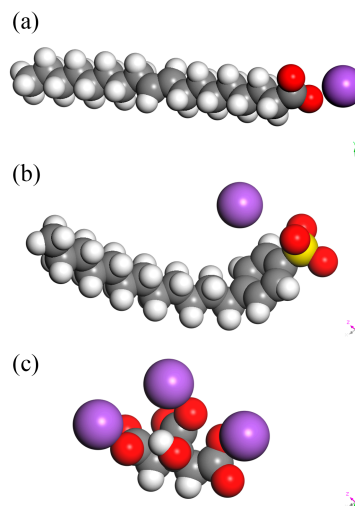


Figure 6. Structure of (a) sodium oleate, (b) SDBS, and (c) sodium citrate. (Note: Red balls represent O. White balls represent H. Yellow balls represent S. Green balls represent Ca. Purple balls represent Na).

3.4. Molecular Dynamics Simulations

Although the intermolecular force is much weaker than the chemical bond, it plays a crucial role in molecular packing and arrangement. Both the stability and the interfacial properties of the molecules depend on the intermolecular forces [50]. The interaction energies between the additives and crystal faces can be used as a quantitative criterion to evaluate the adsorption differences.

Table 2 shows the interaction energies of the additives on parts of the crystal faces including (400), (310), and (530). Different additives on the same face and the same additive on different faces can be compared to illustrate the differences in face growth.

In Table 2, the negative adsorption energies on the face of (400) indicated that sodium oleate, SDBS, and sodium citrate could stably adsorb on the face. The face (400) of the hydrothermal products retained and the characteristic peak could be observed in the XRD patterns. Furthermore, among the three additives, SDBS had the lowest interaction energy with the face of (400), indicating that the adsorption of SDBS on the face was the most stable. The interaction energy of sodium citrate on (310) was $-871.84 \text{ kJ}\cdot\text{mol}^{-1}$, which was much more negative than those of sodium oleate and SDBS. Thus, sodium citrate could adsorb on (310) more stably. Finally, all the faces presented similar growth rates and short columnar or plane products were synthesized in the presence of sodium citrate. As most of the atoms exposed on (310) and (530) were oxygen and hydrogen atoms, the additives could react with calcium atoms by penetrating the oxygen and hydrogen layers. However, the unique functional groups and the long hydrocarbyl groups of sodium oleate and SDBS limited their adsorption on (310) and (530). Compared with the strong interactions on (400), sodium oleate and SDBS could inhibit the growth of (310) and (530) to some extent. The selective adsorption of the additives and the interaction differences caused different crystal growth orientations. As a result, the hydrothermal products presented different morphologies.

Table 2. Interaction energy of additives on predominant crystal faces.

Additive	Interaction Energy ($\text{kJ}\cdot\text{mol}^{-1}$)		
	(400)	(310)	(530)
Sodium oleate	-79.60	-51.28	-68.42
SDBS	-106.16	-73.13	-68.31
Sodium citrate	-59.25	-871.84	-59.91

4. Conclusions

The calcium sulfate whiskers could be prepared from the semi-dry desulfurization residues by hydrothermal synthesis reaction methods. Based on the experimental results of the hydrothermal synthesis reaction, sodium oleate and SDBS facilitate the preparation of calcium sulfate whiskers. Calcium sulfate whiskers with a length of $125 \mu\text{m}$ and an aspect ratio of 41.67 were synthesized with 0.1% (mass ratio to residues) SDBS. Because of the adsorption of the additives, both the surface and the cross-sections of the products were rougher than those without additives.

Considering differences in the structures of crystal faces and that the molecular characteristics of the additives resulted in different adsorption configurations, the adsorption of Ca^{2+} and SO_4^{2-} could be influenced at different levels, which led to significantly different crystal orientation. Based on the XRD patterns of the hydrothermal products, (400), (200), (310), and (530) were identified as the predominant faces.

Employing molecular dynamics simulations, the interaction energies between the additives and the representative faces (400), (310), and (530) were calculated. Among the calculated faces, (400) had the lowest interaction energies with sodium oleate and SDBS, which was indicative of stable adsorption of sodium oleate and SDBS on it. The crystal growth along the c-axis was promoted. However, sodium citrate had the lowest adsorption energy with face (310), which was suggestive of stable adsorption configuration of sodium citrate on (310). No significant enhancement in the crystal growth along the c-axis was observed. As a result, targeted calcium sulfate whiskers with a large aspect ratio could be prepared by adding SDBS. Furthermore, the calculation results were consistent with the XRD patterns, and both results indicated that sodium oleate and SDBS could promote the growth of the rod-like or acicular products.

The present study experimentally realized the utilization of semi-dry desulfurization residues from which calcium sulfate whiskers were prepared, taking advantage of the hydrothermal synthesis

method, with the addition of sodium oleate and SDBS. Based on this study, further insights into the controlling mechanism of the additives on the hydrothermal products, as well as the specified adsorption quantity of the additives, will be carried out in the following study, aiming to improve the quality and the homogeneity of the prepared calcium sulfate whiskers.

Author Contributions: Conceptualization, Methodology, and Writing—Review & Editing, L.L. and Z.Y.; Software, Formal Analysis, Investigation, and Writing—Original Draft Preparation, H.H.; Supervision and Funding Acquisition, L.L.; Project Administration, Z.Y.

Funding: This study was financially supported by the National Natural Science Foundation of China (No. 51574061).

Acknowledgments: The authors gratefully acknowledge the financial supports by the National Science Foundation of China, as well as the China Scholarship Council (201706080110).

Conflicts of Interest: The authors declare no conflict of interest.

References

1. Liu, R.; Guo, B.; Ren, A.; Bian, J. The chemical and oxidation characteristics of semi-dry flue gas desulfurization ash from a steel factory. *Waste Manag. Res.* **2009**, *28*, 865–871. [[CrossRef](#)] [[PubMed](#)]
2. Castro, R.d.P.V.d.; Medeiros, J.L.d.; Araújo, O.d.Q.F.; Cruz, M.d.A.; Ribeiro, G.T.; Oliveira, V.R.d. Fluidized bed treatment of residues of semi-dry flue gas desulfurization units of coal-fired power plants for conversion of sulfites to sulfates. *Energy Convers. Manag.* **2017**, *143*, 173–187. [[CrossRef](#)]
3. Chen, Z.; Wu, S.; Li, F.; Chen, J.; Qin, Z.; Pang, L. Recycling of flue gas desulfurization residues in gneiss based hot mix asphalt: Materials characterization and performances evaluation. *Constr. Build. Mater.* **2014**, *73*, 137–144. [[CrossRef](#)]
4. Clark, R.B.; Ritchey, K.D.; Baligar, V.C. Benefits and constraints for use of fgd products on agricultural land. *Fuel* **2001**, *80*, 821–828. [[CrossRef](#)]
5. Solem-Tishmack, J.K.; McCarthy, G.J.; Docktor, B.; Eylands, K.E.; Thompson, J.S.; Hassett, D.J. High-calcium coal combustion by-products: Engineering properties, ettringite formation, and potential application in solidification and stabilization of selenium and boron. *Cem. Concr. Res.* **1995**, *25*, 658–670. [[CrossRef](#)]
6. Srisomang, R.; Naksata, W.; Thiansem, S.; Sooksamiti, P.; Arqueropanyo, O.-A. Utilization of leonardite, flue gas desulfurization gypsum and clay for production of ceramic plant growth material. *Environ. Earth Sci.* **2015**, *73*, 1621–1628. [[CrossRef](#)]
7. Telesca, A.; Marroccoli, M.; Calabrese, D.; Valenti, G.L.; Montagnaro, F. Flue gas desulfurization gypsum and coal fly ash as basic components of prefabricated building materials. *Waste Manag.* **2013**, *33*, 628–633. [[CrossRef](#)] [[PubMed](#)]
8. Wang, Y.; Shi, L. The effects of modified flue gas desulfurization residue on growth of sweet potato and soil amelioration. *Water Air Soil Pollut.* **2015**, *226*, 245. [[CrossRef](#)]
9. Burgess-Conforti, J.R.; Brye, K.R.; Miller, D.M.; Pollock, E.D.; Wood, L.S. Dry flue gas desulfurization by-product application effects on plant uptake and soil storage changes in a managed grassland. *Environ. Sci. Pollut. Res.* **2018**, *25*, 3386–3396. [[CrossRef](#)] [[PubMed](#)]
10. Ren, L.; Wang, W.; Ma, C.; Xu, X.; Dong, Y. Study on a new utilization method for dry and semi-dry desulfurization fdg residues. In Proceedings of the 2009 Asia-Pacific Power and Energy Engineering Conference, Wuhan, China, 28–31 March 2009; pp. 1–5.
11. Chai, N.; Shi, L.; Li, J. Amelioration of acidic soil using the calcined product of dry and semi-dry desulfurization residue with k-feldspar: Plant and soil responses and heavy metal assessment. In Proceedings of the 2010 4th International Conference on Bioinformatics and Biomedical Engineering, Chengdu, China, 18–20 June 2010; pp. 1–5.
12. Li, Y.; Jing, P.; Zhou, J.; Zhu, T. Calcium sulfite oxidation and crystal growth in the process of calcium carbide residue to produce gypsum. *Waste Biomass Valoriz.* **2014**, *5*, 125–131. [[CrossRef](#)]
13. Xu, A.; Li, H.; Luo, K.; Xiang, L. Formation of calcium sulfate whiskers from caco₃-bearing desulfurization gypsum. *Res. Chem. Intermed.* **2011**, *37*, 449–455. [[CrossRef](#)]
14. Yang, L.; Wang, X.; Zhu, X.; Du, L. *Preparation of Calcium Sulfate Whisker by Hydrothermal Method from Flue Gas Desulfurization (fgd) Gypsum*; Trans Tech: London, UK, 2013; pp. 823–826.

15. Li, J.; Zhuang, X.; Querol, X.; Font, O.; Moreno, N. A review on the applications of coal combustion products in china. *Int. Geol. Rev.* **2018**, *60*, 671–716. [[CrossRef](#)]
16. Tan, H.; Dong, F.; Liu, J. Morphology control of calcium sulfate hemihydrates and application in size screening iron/sulfur of jarosite sediment. *J. Phys. Chem. Solids* **2018**, *112*, 239–245. [[CrossRef](#)]
17. Wang, X.; Wang, L.; Wang, Y.; Tan, R.; Ke, X.; Zhou, X.; Geng, J.; Hou, H.; Zhou, M. Calcium sulfate hemihydrate whiskers obtained from flue gas desulfurization gypsum and used for the adsorption removal of lead. *Crystals* **2017**, *7*, 270. [[CrossRef](#)]
18. Sun, H.; Tan, D.; Peng, T.; Liang, Y. Preparation of calcium sulfate whisker by atmospheric acidification method from flue gas desulfurization gypsum. *Proced. Environ. Sci.* **2016**, *31*, 621–626. [[CrossRef](#)]
19. Wang, X.; Yang, L.; Zhu, X.; Yang, J. Preparation of calcium sulfate whiskers from fgd gypsum via hydrothermal crystallization in the H₂SO₄–NaCl–H₂O system. *Particuology* **2014**, *17*, 42–48. [[CrossRef](#)]
20. Liu, T.; Fan, H.; Xu, Y.; Song, X.; Yu, J. Effects of metal ions on the morphology of calcium sulfate hemihydrate whiskers by hydrothermal method. *Front. Chem. Sci. Eng.* **2017**, *11*, 545–553. [[CrossRef](#)]
21. Feng, X.; Zhang, Y.; Wang, G.; Miao, M.; Shi, L. Dual-surface modification of calcium sulfate whisker with sodium hexametaphosphate/silica and use as new water-resistant reinforcing fillers in papermaking. *Powder Technol.* **2015**, *271*, 1–6. [[CrossRef](#)]
22. Yuan, W.; Cui, J.; Cai, Y.; Xu, S. A novel surface modification for calcium sulfate whisker used for reinforcement of poly(vinyl chloride). *J. Polym. Res.* **2015**, *22*, 173. [[CrossRef](#)]
23. Wang, H.; Mu, B.; Ren, J.; Jian, L.; Zhang, J.; Yang, S. Mechanical and tribological behaviors of pa66/pvdf blends filled with calcium sulphate whiskers. *Polym. Compos.* **2009**, *30*, 1326–1332. [[CrossRef](#)]
24. Wang, J.; Pan, X.C.; Xue, Y.; Cang, S.J. Studies on the application properties of calcium sulfate whisker in silicone rubber composites. *J. Elastomers Plast.* **2011**, *44*, 55–66. [[CrossRef](#)]
25. Yang, J.; Nie, S.; Zhu, J. Fabrication and characterization of poly(lactic acid) biocomposites reinforced by calcium sulfate whisker. *J. Polym. Environ.* **2018**, *26*, 3458–3469. [[CrossRef](#)]
26. Wang, J.; Yang, K.; Lu, S. Preparation and characteristic of novel silicone rubber composites based on organophilic calcium sulfate whisker. *High Perform. Polym.* **2011**, *23*, 141–150. [[CrossRef](#)]
27. Pan, Z.; Lou, Y.; Yang, G.; Ni, X.; Chen, M.; Xu, H.; Miao, X.; Liu, J.; Hu, C.; Huang, Q. Preparation of calcium sulfate dihydrate and calcium sulfate hemihydrate with controllable crystal morphology by using ethanol additive. *Ceram. Int.* **2013**, *39*, 5495–5502. [[CrossRef](#)]
28. Liu, C.; Zhao, Q.; Wang, Y.; Shi, P.; Jiang, M. Hydrothermal synthesis of calcium sulfate whisker from flue gas desulfurization gypsum. *Chin. J. Chem. Eng.* **2016**, *24*, 1552–1560. [[CrossRef](#)]
29. Liu, C.; Zhao, Q.; Wang, Y.; Shi, P.; Jiang, M. Surface modification of calcium sulfate whisker prepared from flue gas desulfurization gypsum. *Appl. Surf. Sci.* **2016**, *360*, 263–269. [[CrossRef](#)]
30. Yang, N.; Xiao, H.; Guo, W. Additives-assisted hydrothermal synthesis of calcium sulfate whisker and its growth mechanism. *J. Chin. Ceram. Soc.* **2014**, *42*, 539–544.
31. Kong, B.; Guan, B.; Yates, M.Z.; Wu, Z. Control of α -calcium sulfate hemihydrate morphology using reverse microemulsions. *Langmuir* **2012**, *28*, 14137–14142. [[CrossRef](#)] [[PubMed](#)]
32. Zhou, P.; Wu, H.; Xia, Y. Influence of synthetic polymers on the mechanical properties of hardened β -calcium sulfate hemihydrate plasters. *J. Ind. Eng. Chem.* **2016**, *33*, 355–361. [[CrossRef](#)]
33. Chen, R.; Hou, S.; Wang, J.; Xiang, L. Influence of alkyl trimethyl ammonium bromides on hydrothermal formation of α -CaSO₄·0.5H₂O whiskers with high aspect ratios. *Crystals* **2017**, *7*, 28. [[CrossRef](#)]
34. Poornachary, S.K.; Chow, P.S.; Tan, R.B.H. Impurity effects on the growth of molecular crystals: Experiments and modeling. *Adv. Powder Technol.* **2008**, *19*, 459–473. [[CrossRef](#)]
35. Clydesdale, G.; Thomson, G.B.; Walker, E.M.; Roberts, K.J.; Meenan, P.; Docherty, R. A molecular modeling study of the crystal morphology of adipic acid and its habit modification by homologous impurities. *Cryst. Growth Des.* **2005**, *5*, 2154–2163. [[CrossRef](#)]
36. Hadicke, E.; Rieger, J.; Ursula Rau, I.; Boeckh, D. Molecular dynamics simulations of the incrustation inhibition by polymeric additives. *Phys. Chem. Chem. Phys.* **1999**, *1*, 3891–3898. [[CrossRef](#)]
37. Guan, Q.; Hu, Y.; Tang, H.; Sun, W.; Gao, Z. Preparation of α -CaSO₄· $\frac{1}{2}$ H₂O with tunable morphology from flue gas desulphurization gypsum using malic acid as modifier: A theoretical and experimental study. *J. Colloid Interface Sci.* **2018**, *530*, 292–301. [[CrossRef](#)] [[PubMed](#)]
38. Yani, Y.; Chow, P.S.; Tan, R.B.H. Molecular simulation study of the effect of various additives on salbutamol sulfate crystal habit. *Mol. Pharm.* **2011**, *8*, 1910–1918. [[CrossRef](#)] [[PubMed](#)]

39. Mao, X.; Song, X.; Lu, G.; Xu, Y.; Sun, Y.; Yu, J. Effect of additives on the morphology of calcium sulfate hemihydrate: Experimental and molecular dynamics simulation studies. *Chem. Eng. J.* **2015**, *278*, 320–327. [[CrossRef](#)]
40. Chakraborty, T.; Hens, A.; Kulashrestha, S.; Chandra Murmu, N.; Banerjee, P. Calculation of diffusion coefficient of long chain molecules using molecular dynamics. *Physica E* **2015**, *69*, 371–377. [[CrossRef](#)]
41. Bezou, C.; Nonat, A.; Mutin, J.C.; Christensen, A.N.; Lehmann, M.S. Investigation of the crystal structure of γ -CaSO₄, CaSO₄ · 0.5 H₂O, and CaSO₄ · 0.6 H₂O by powder diffraction methods. *J. Solid State Chem.* **1995**, *117*, 165–176. [[CrossRef](#)]
42. Kitao, O.; Miura, N.; Ushiyama, H. Molecular mechanics with qeq-cs (charge equilibration method generalized for charge separation system) dedicated to professor keiji morokuma in celebration of his 65th birthday.1. *J. Mol. Struct. Theochem* **1999**, *461–462*, 239–247. [[CrossRef](#)]
43. Wang, L.; Liu, G.; Song, X.; Yu, J. Molecular modeling for selective adsorption of halite with dodecylmorpholine. *Acta Phys.-Chim. Sin.* **2009**, *25*, 963–969.
44. Feldmann, T.; Demopoulos, G.P. Effects of crystal habit modifiers on the morphology of calcium sulfate dihydrate grown in strong CaCl₂-HCl solutions. *J. Chem. Technol. Biotechnol.* **2014**, *89*, 1523–1533. [[CrossRef](#)]
45. Orme, C.A.; Noy, A.; Wierzbicki, A.; McBride, M.T.; Grantham, M.; Teng, H.H.; Dove, P.M.; DeYoreo, J.J. Formation of chiral morphologies through selective binding of amino acids to calcite surface steps. *Nature* **2001**, *411*, 775. [[CrossRef](#)] [[PubMed](#)]
46. Shen, Z.; Guan, B.; Fu, H.; Yang, L. Effect of potassium sodium tartrate and sodium citrate on the preparation of α -calcium sulfate hemihydrate from flue gas desulfurization gypsum in a concentrated electrolyte solution. *J. Am. Ceram. Soc.* **2009**, *92*, 2894–2899. [[CrossRef](#)]
47. Addala, S.; Bouhdjer, L.; Chala, A.; Bouhdjar, A.; Halimi, O.; Boudine, B.; Sebais, M. Structural and optical properties of a nacl single crystal doped with cuo nanocrystals. *Chin. Phys. B* **2013**, *22*, 098103. [[CrossRef](#)]
48. Rai, R.; Triloki, T.; Singh, B.K. X-ray diffraction line profile analysis of kbr thin films. *Appl. Phys. A* **2016**, *122*, 774. [[CrossRef](#)]
49. Tang, Y.; Gao, J. Investigation of the effects of sodium dicarboxylates on the crystal habit of calcium sulfate α -hemihydrate. *Langmuir* **2017**, *33*, 9637–9644. [[CrossRef](#)] [[PubMed](#)]
50. Wei, C.; Huang, H.; Duan, X.; Pei, C. Structures and properties prediction of hmx/tatb co-crystal. *Propellants, Explos. Pyrotech.* **2011**, *36*, 416–423. [[CrossRef](#)]



© 2018 by the authors. Licensee MDPI, Basel, Switzerland. This article is an open access article distributed under the terms and conditions of the Creative Commons Attribution (CC BY) license (<http://creativecommons.org/licenses/by/4.0/>).